Journal of Petroleum Science and Technology 15(1): 45, 2025, Pages 15-25
DOI:10.22078/jpst.2026.5818.1994

Journal of Petroleum Science and Technology
Research Paper
https://jpst.ripi.ir/

Extending Dual Porosity Models to Anisotropic Fractured Reservoirs Using Physics-Guided Neural Networks

Mohsen Masihi*[1], Mohammad Zaree[1], Ali Salehi[1], Qingrong Xiong[2]
1. Department of Chemical and Petroleum Engineering, Sharif University of Technology, Iran
2. School of Civil Engineering, Shandong University, China

Abstract
The non-orthogonal fractures in conventional Warren and Root (WR) induce directional permeabilities and anisotropic flow patterns that cannot be captured using simple fracture properties. In this paper, we use the proposed equivalent fracture aperture, obtained via a correction coefficient (η), to account for this effect. Previous studies estimated this coefficient by calibrating to static field data. The main contribution is to treat this coefficient as a physics-dependent parameter rather than a calibration value to bridge fracture-scale flow with the continuum model. A data-driven approach is developed to quantify η as a function of fracture geometry and reservoir-scale properties. Moreover, a dataset of 2,478 simulation samples was generated using COMSOL Multiphysics, covering a range of fracture and reservoir properties. In addition, an artificial neural network (ANN) was trained and optimized on this dataset to learn the nonlinear relation with the correction coefficient, achieving a predictive accuracy of $R^2 = 0.9946$. By using the ANN-predicted correction coefficient in the WR approach, a multiscale bridge between fracture-scale physics and dual-porosity models can be achieved. Furthermore, the cubic relationship between permeability and fracture aperture ($k_\theta = \eta^3 k$) highlights the importance of accurate η estimation, as any error in η propagates results into large permeability uncertainties. Ultimately, the numerical results showed that the dependency of the correction coefficient η on fracture orientation is much greater than its dependency on either fracture size and matrix shape or system size. Also, using this simple correction factor, the applicability of conventional dual-porosity models to anisotropic fractured reservoirs with non-orthogonal fractures is extended. .

Keywords: Naturally Fractured Reservoirs, Anisotropy, Artificial Neural Network, Fracture Aperture Correction Coefficient.

Introduction
Understanding fluid flow behavior in naturally fractured reservoirs is important for designing an appropriate reservoir development scenario and increasing hydrocarbon recovery, as fractures act as preferential pathways for fluid flow. Moreover, fractured reservoirs consist of two interacting low-permeability matrices and a high-permeability fracture medium. In addition, fractures introduce significant anisotropy due to their spatial distribution and orientation, thereby yielding different permeability values in different directions. Fractured reservoirs are classified based on the fracture and matrix permeability ratio [1], the differences in rock properties [2], or the capacity for fluid storage and their interconnection [3]. However, these classifications often neglect anisotropy, which plays a key role in designing an appropriate reservoir development scenario. The contribution of each fracture or set of fractures depends on parameters such as aperture, size, orientation, density, connectivity, and filling material, all of which affect the flow behavior. Fracture orientation, i.e., dip and strike, controls the reservoir anisotropy. Moreover, fracture size influences rock permeability [4], and the condition of fracture walls and fracture-filling details (i.e., the type and amount of sedimentary material) affect flow behavior at the fracture scale. Moreover, fracture density or spacing, which is related to the degree of rock fracturing, is essential for the main flow [5]. Fracture aperture—the perpendicular distance between fracture walls—strongly influences both porosity and permeability, and it varies with depth, in-situ stress, lithology, and pore pressure [6]. Fracture permeability (kf) depends on the aperture by (as seen in Equation 1),

$$k_f = \frac{b^2}{12} cos^2(\alpha) \quad (1)$$

**Corresponding author:* Mohsen Masihi, *Department of Chemical and Petroleum Engineering, Sharif University of Technology, Iran*
E-mail addresses: masihi@sharif.edu
Received 2025-12-21, Received in revised form 2026-06-10, Accepted 2026-06-13, Available online .....

where b is fracture aperture and α is the fracture angle relative to the flow direction [7]. Similarly, fracture porosity, in the case of the Warren and Root (WR) model, depends linearly on the aperture by (as seen in Equation 2),

$$\phi \approx b\left(\frac{1}{a_1}+\frac{1}{a_2}+\frac{1}{a_3}\right) \quad (2)$$

Previous studies indicate a cubic relationship between rock porosity and permeability in single-phase flow [8]; Lucia [9-10]. However, for multi-phase flow, other complementary functions, including relative permeability and capillary pressure, are needed [11].

Modeling flow through fractured porous media can be performed by using various approaches. The first method is to use a discrete fracture network (DFN) by which fractures randomly distributed in the medium are explicitly represented as 2D line segments or 3D shapes [12-14]. On the other hand, continuum models such as dual-porosity or multi-porosity models treat fractures and matrix as two overlapping continua with possible flow exchange between them [15-16]. However, to apply this approach in real-world cases, we need appropriate parameter calibration to account for anisotropy and local heterogeneity. Furthermore, the continuum approaches have been extended by many researchers, including Kazemi [17-19], with a focus on improving numerical methods (e.g., finite-difference discretization) or analyzing the gravity and mobility terms. Another publication used coupling terms to enhance flow exchange in fractured porous media [20,5]. The continuum models are computationally efficient methods, especially for multiphase flow, but their results will be questionable if fractures are not interconnected [14, 21,2]. In some studies, discrete fracture models have been used to evaluate transfer functions between the two media in continuum models. As an example, dual-porosity models have been used to assess CO_2 storage potential in a fractured reservoir by analyzing the fracture system [22]. Another dual-porosity model for geothermal fractured reservoirs considered convective flow faster [6]. In another study, an improved dual-porosity-dual-permeability model was used, which enhanced the accuracy of flow modeling [23].

COMSOL Multiphysics can be used to simulate flow through porous media under various displacement mechanisms. For direct pore-scale simulations, it employs the main flow equations (Navier-Stokes) coupled with interface tracking algorithms [24]. The flow equations are solved using finite element, finite volume, or boundary element methods, along with algorithms like level set or phase field to track the fluid interfaces [25-27] investigated the relative changes in porosity, permeability, and elastic modulus through single-phase flow in fractured media using coupled hydrodynamic and geomechanical models [28]. It is observed that the streamlines are influenced by (1) fracture orientation, (2) well distance, and (3) fracture density. Also, [29]. conducted COMSOL simulations to analyze viscous fingering in porous media, using the Brinkman equation for non-Darcy cases [29]. Recent advancements have further oriented the analysis of flow in fracture networks. For instance, [30] employed probabilistic assessments of equivalent fracture aperture constrained by real-time drilling mud loss data. Additionally, [31] developed a phase-field model in COMSOL for fluid-driven dynamic crack propagation in porous media, providing insights into the interaction between fluid flow and fracture development.

Furthermore, machine learning techniques have been applied to enhance fracture characterization and to improve simulation performance. For instance, El Ouahed et al. developed a 2D fracture-intensity map and network in the Hassi Messaoud field using artificial neural networks (ANNs) and fuzzy logic, demonstrating AI's potential to predict fracture zones from well data [32]. Similarly, Al-Dhamen et al. proposed an AI-based model to estimate acid fracturing performance in naturally fractured reservoirs, offering a computationally efficient approach compared with traditional simulations [33]. In another study, Peng et al. considered embedded discrete fractures, along with AI, for history matching in fractured reservoirs [34]. Furthermore, other approaches, such as support vector machines (SVM), have been coupled with neural networks to identify fractures in shale gas reservoirs [35]. Moreover, AI methods, coupled with reservoir simulations, have been applied to generate simulation cases to characterize fracture properties in shale gas reservoirs [36]. Lastly, techniques such as random forests and neural networks have been used to predict complex fluid-flow behavior and to address fluid losses in fractured reservoirs [37-38] utilized machine learning to study the role of a single fracture in fractured dolomite formations. Recent ANN models in fractured reservoirs emphasize their suitability for capturing complex nonlinearities in fracture flow [39-40].

Fractures as heterogeneous media create anisotropic flow patterns. For anisotropy representation in fractured porous media, the use of an equivalent aperture from a realistic aperture distribution or of stress-aperture relations in the medium has been proposed [21, 22, 41]. For example, Young et al [21] proposed an equivalent fracture aperture to account for the anisotropic flow patterns in terms of the permeability tensor. However, their approach focuses only on fracture orientation and ignores the matrix shape. Moreover, Nick and Bisdom (2018) emphasized that using a constant aperture for the fracture network may not reproduce the true permeability anisotropy. Zhang et al. [22] recently applied this concept to coalbed methane reservoirs, showing improved consistency with field data. They found that incorporating such an anisotropic correction factor into WR models more accurately represents directional permeability and reservoir behavior. However, the considerable uncertainty in the spatial distribution of fractures and the scarcity of fracture data may affect their estimate of this correction factor. To overcome this effect, we combine COMSOL-based numerical simulation results with an appropriate artificial neural network (ANN) to estimate the fracture aperture correction coefficient for anisotropic fractured reservoirs. By incorporating this coefficient, which represents directional flow behavior, the proposed correction extends the applicability of dual-porosity WR models to anisotropic reservoirs.

Materials and Methods

Characterization and Physical Properties of Fractured Rocks

Hydrocarbons in fractured reservoirs primarily reside within matrix pore networks, whereas fluid transport to production

wells occurs primarily through interconnected fracture systems. Fracture networks possess various attributes, such as aperture dimensions, spatial extent, orientation patterns, distribution density, intensity variations, connectivity characteristics, and spatial correlations [42-43]. Accurate reservoir characterization and performance prediction require a thorough understanding of (1) fracture-influenced rock properties, (2) particularly compressibility, (3) permeability tensors, (4) effective porosity, (5) capillary pressure curves, and (6) wettability alterations. These properties exhibit significant heterogeneity depending on fracture attributes and spatial configurations, leading to complex flow behavior that conventional models often struggle to capture. To investigate these complex interactions, we investigate two distinct flow scenarios: (1) single-phase fluid transport through fractured porous media with fractures oriented at different inclination angles relative to the primary flow direction, and (2) two-phase immiscible water-oil displacement in fractured systems with systematically varied fracture inclinations. This section elucidates the theoretical basis of flow modeling in fractured media, outlines the assumptions of our base model formulation, and describes the numerical simulation methodology used to address these multiscale, coupled phenomena.

Single-Phase Fluid Flow in a Porous Medium with Fractures

The governing equations for single-phase fluid flow in a fractured porous medium are given by,

For matrix (as seen in Equation 3):

$$\frac{\partial(\varphi\rho)}{\partial t}=-\nabla.(\rho u)-q_{mf} \quad (3)$$

For fractures (as seen in Equation 4):

$$\frac{\partial(\varphi_f\ \rho_f\ )}{\partial t}=-\nabla.(\rho_f\ u_f\ )+q_{mf}+q_{ext} \quad (4)$$

where the term q_mf represents the fluid transfer between the matrix and fractures is calculated by Equation 5:

$$q_{mf}=\alpha_w\ (p_{matrix}-p_{fracture}) \quad (5)$$

α_w is the fluid transfer function, the porosity is denoted by ϕ, the fluid density per unit volume by ρ, the Darcy superficial velocity by u = (u_1،u_2،u_3), and external sources and sinks by q, k is the absolute permeability tensor of the porous medium, μ is the fluid viscosity, g is the gravitational acceleration, z is the depth, and ∇ is the gradient operator.

Two-Phase Fluid Flow in a Porous Medium with Fractures

For immiscible two-phase flow (water and oil), the governing transport equations are:

-for fracture (as seen in Equation 6):

$$\varphi_f\ \frac{\partial(S_{\alpha f})}{\alpha t}+\nabla.u_f=+\tau_\alpha=+T_\alpha(\psi_{\alpha m}-\psi_{\alpha f}) \quad (6)$$

- for matrix (as seen in Equation 7):

$$\varphi_f\ \frac{\partial(S_{\alpha f}\ )}{\partial t}+\nabla.u_{\alpha f}=+\tau_\alpha=+T_\alpha\ (\psi_{\alpha m}-\psi_{\alpha f}) \quad (7)$$

where S_α is phase saturation, $\psi_\alpha=p_\alpha-\rho g\Delta z$ is flow potential, and T is the matrix transmissibility coefficient, with the subscript α indicating the water or oil phase.

The transfer function is defined as follows:

For oil (as calculated using Equation 8):

$$\tau_o=\frac{\alpha K_m\ K_{ro}}{\mu_o\ B_o}(\psi_{om}-\psi_{of}) \quad (8)$$

For water (as calculated using Equation 9):

$$\tau_w=\frac{\alpha K_m\ K_{rw}}{\mu_w\ B_w}(\psi_{wm}-\psi_{wf}) \quad (9)$$

Fracture Aperture, Porosity, and Equivalent Permeability

The classical Warren-Root (WR) model assumes orthogonal fracture networks with uniform apertures, which limit its applicability for fractures inclined relative to the flow direction. To address this limitation, the approach introduced by Yang et al. [44] can be used. This approach incorporates an exponential correction factor η to adjust fracture apertures and account for the anisotropy effects (as seen in Equation 10):

$$b_\theta=\eta b \quad (10)$$

where b is the base fracture aperture, $b\theta$ is the fracture aperture in an anisotropic system with fractures at an angle θ relative to the main flow and η is a coupling parameter between the geometry and flow. Considering non-orthogonal fractures relative to the main flow direction enhances fracture connectivity and the medium's conductivity. This improvement in the flowability may be represented by an increase in the fracture aperture; hence, we expect the aperture correction factor η to have some values greater than 1. However, the detailed dependency of this parameter on fracture orientation, θ, is not clear as the size of the fracture projection along the main flow is decreased with fracture orientation.

Porosity and permeability can then be adjusted accordingly, with porosity scaling linearly $\eta\varphi$, and permeability scaling cubically;

$$k_\theta=\eta^3\ k \quad (11)$$

This correction improves the application of dual-porosity models in simulating anisotropic fractured reservoirs [22, 45].

Numerical Model Setup

A comprehensive two-phase (oil-water) flow model was implemented in COMSOL Multiphysics to investigate immiscible fluid displacement mechanisms in heterogeneous, fractured porous media. Moreover, the computational domain consisted of a two-dimensional reservoir section (120 m × 50 m) where fractures were explicitly represented as discrete line segments with systematically varied orientations and spacing to effectively capture the inherent anisotropic flow behavior. The ratio of reservoir size to matrix block size, 4 to 28, is considered representative of fracture-matrix interactions in the medium. Moreover, the fracture orientation distribution spanned 5 to 90 degrees, providing a range of anisotropies in permeability. The multiphase transport phenomena were simulated through the Multiphase Flow in Porous Media interface, which integrates Darcy's Law with Phase Transport equations to resolve the coupled pressure-saturation dynamics at both fracture and matrix scales.

This investigation specifically focused on the influence of fracture network geometry on displacement efficiency and flow anisotropy. Multiple numerical experiments were conducted with fracture systems configured at two principal orientations and systematically varied matrix block dimensions to examine scale-dependent behaviors. For each configuration, the spatiotemporal evolution of fluid

pressures was monitored at discrete points throughout the fracture network, enabling the calculation of the volume-averaged pressure distribution across the entire fracture system at each time step. Furthermore, we quantitatively assessed the impact of an empirical correction factor on critical performance indicators, including oil saturation profiles within fractures, water saturation distribution within the matrix domain, and fluid velocity distributions along the outflow boundary.

The governing parameters and constitutive relationships utilized in the numerical simulations are comprehensively summarized in Table 1. The Brooks-Corey formulation was implemented to characterize the relative permeability functions and capillary pressure-saturation relationships for the two-phase system. Moreover, this constitutive model provides a robust framework for quantifying the nonlinear dependence of relative permeability on normalized water saturation and establishes the functional relationship between capillary pressure and fluid saturation in heterogeneous porous media. For the compressible storage calculations, a linearized storage model was employed that incorporates both fluid compressibility and rock compressibility coefficients, thus accounting for the total storage capacity of the fractured porous medium under transient pressure conditions.

Discrete fractures were incorporated into the rectangular computational domain as explicit line segments with precisely controlled orientations and spatial distributions to represent the heterogeneous reservoir architecture. The governing equations for fluid transport were implemented by applying Darcy's Law physics module throughout the entire domain, with fractures systematically integrated as distinct geometric features within this physics interface to capture their unique flow characteristics. Each fracture element was parameterized with specified physical properties, including aperture dimensions, effective porosity, intrinsic permeability tensor, and mechanical compressibility, based on the calibrated values presented in Table 1.

The hydraulic boundary conditions were carefully defined to reflect realistic reservoir conditions: constant wellbore pressure boundaries were set at designated production/injection locations, while fluid outflow constraints were applied within the Phase Transport physics module at corresponding boundary segments to maintain mathematical consistency.

The computational domain was discretized using an adaptive, physics-controlled finite element mesh consisting of triangular elements with local refinement near fracture interfaces and in regions of anticipated high-pressure gradients to ensure numerical accuracy and stability. Moreover, mesh sensitivity analyses were conducted to establish mesh independence, confirming that the selected discretization adequately resolved the multiscale transport phenomena without introducing numerical artifacts. In addition, the transient simulations were executed over a 100-day production period using progressive daily time-stepping with automatic time-step adjustment to efficiently capture both early-time rapid dynamics and late-time quasi-steady behavior. Furthermore, this comprehensive numerical approach enables robust characterization of the complex, coupled processes governing multiphase flow in fractured reservoirs while maintaining computational efficiency.

Artificial Intelligence-Based Estimation of Fracture Aperture Correction Coefficient

Data Preparation

A dataset of 2,478 samples was generated by running COMSOL simulations. Moreover, different fracture angles, matrix sizes, and other rock/fluid properties were assumed to capture realistic fracture flow behavior. These data are stored in a CSV file. The initial dataset comprises multiple simulation-derived samples, each representing a unique combination of input conditions under controlled settings. Also, data preprocessing was conducted to address common machine learning challenges, such as overfitting, noise sensitivity, and scale-related biases, in order to ensure data quality, consistency, and compatibility with the machine learning model:

1. **Data Loading and Selection**: The dataset is loaded from the CSV file, with the first three columns designated as input features (X) and the fourth column as the target output (y). In addition, the dataset's initial size is verified to confirm the data's structure and integrity.

2. **Outlier Removal**: Outliers are identified and removed using the Z-score method, with a threshold of 1.7. Furthermore, removing outliers makes the dataset more robust to erroneous simulation outputs. Samples where all features have a Z-score below this threshold are retained, while others are discarded.

Table 1 The input parameters for the constructed model.

Input Parameter	Value	Unit	Input Parameter	Value	Unit
Reservoir Dimensions	120 x 50	m^2	Water Viscosity	1	cP
Initial Reservoir Pressure	2	MPa	Water Compressibility	4.00e-10	1/Pa
Initial Oil Saturation	0.7	-	Matrix Porosity	0.15	-
Residual Oil Saturation	0.2	-	Matrix Permeability	2.00e-12	m^2
Residual Water Saturation	0	-	Matrix Compressibility	1.00e-4	1/Pa
Perforated Zone	30	m	Initial Fracture Aperture	0.02	m
Wellbore Pressure	6	atm	Fracture Porosity	1	-
Oil Density	800	kg/m^3	Fracture Permeability	1.00e-7	m^2
Oil Viscosity	1.5	cP	Fracture Compressibility	1.00e-4	1/Pa
Oil Compressibility	4.00e-10	1/Pa			
Water Density	1000	kg/m^3			

This step reduces the dataset size but enhances its quality by eliminating anomalous data points that could skew model performance. After outlier removal, a statistical summary is computed, including metrics such as minimum, maximum, mean, median, variance, and standard deviation. This summary provides insights into the data distribution and ensures the dataset remains representative of the underlying physical phenomena.

3. **Normalization**: To improve the neural network's training efficiency and prevent features with larger scales from dominating the model and ensure numerical stability during training, both input features and the target output are normalized to the range [0, 1] using the Min-Max Scaler. In addition, this normalization ensures that all features contribute equally to the model's learning process, regardless of their original scales.

4. **Data Splitting**: The normalized dataset is split into training (85%) and testing (15%) sets using the train_test_ split function from Scikit-learn, with a fixed random seed (random_state=42) to guarantee that the model is evaluated on a representative subset of the data. The training set is used to fit the neural network, while the testing set is used to evaluate its generalization performance on unseen data.

5. **Statistical Validation**: Post-preprocessing, a detailed statistical analysis was also performed to confirm the dataset's suitability for training. The number of samples in the training and testing sets is reported (approximately 85% and 15% of the filtered dataset, respectively), ensuring sufficient data for robust model training. The statistical summary, including variance and standard deviation, is visualized to verify that the data distribution aligns with expectations for the modeled physical system.

The resulting preprocessed dataset is therefore suitable for training a neural model to capture the nonlinear dependence of the fracture aperture correction coefficient on fracture geometry and reservoir-scale parameters. The preprocessing steps collectively ensure that the data are clean, normalized, and appropriately structured, laying a strong foundation for accurate and reliable model predictions.

Artificial Neural Network (ANN) Modeling

Artificial Neural Networks (ANNs) are computational models designed to identify complex patterns and relationships within data [46]. ANNs consist of interconnected nodes, or neurons, organized into layers: an input layer that accepts data, hidden layers that process it, and an output layer that generates predictions or classifications. Each neuron combines inputs with weights and biases, applies an activation function like ReLU, and produces an output [46]. Training an ANN involves adjusting weights through backpropagation and optimization algorithms, such as gradient descent, to minimize a loss function [46]. ANNs handle noisy data, scale with large datasets, and adapt to complex problems [47]. However, challenges such as overfitting, computational demands, and interpretability issues are common and are often addressed through regularization, dropout, or early stopping [46]. Moreover, ANNs are widely used for pattern recognition, predictive modeling, and data-driven decision-making in engineering and beyond [47].

Artificial Neural Networks (ANNs) were selected for this study due to their ability to approximate nonlinear response surfaces in low-dimensional and physics-driven problems. In the present application, the objective is not to replace physical modeling but to capture the implicit relationship between fracture-scale flow behavior and the equivalent aperture correction coefficient derived from numerical simulations. Given the limited number of input parameters and the nature of η, a shallow feedforward ANN architecture was adopted to balance model expressiveness, interpretability, and generalization capability. A feedforward ANN using TensorFlow and Keras for a regression task was constructed with:

• **Input layer**: 3 nodes corresponding to (1) fracture angle, (2) matrix block size, and (3) reservoir area are used. We use these input parameters as i) the structure of WR models, as continuum models assume full connections among fractures in the medium, ii) the other controlling parameters in WR models, such as fracture density, fracture spacings depend on the matrix block size, and iii) other small-scale ingredients, such as roughness variations in the fractures, are usually ignored in large-scale field simulations.

• **One hidden layer**: 25 neurons with ReLU activation (optimized via sensitivity analysis as shown in Fig. 1).

• **Output layer**: 1 node with a linear activation function representing the correction coefficient η. The model is compiled with the Adam optimizer (learning rate of 0.01) and Mean Squared Error loss function, which measures the squared differences between predicted and actual values.

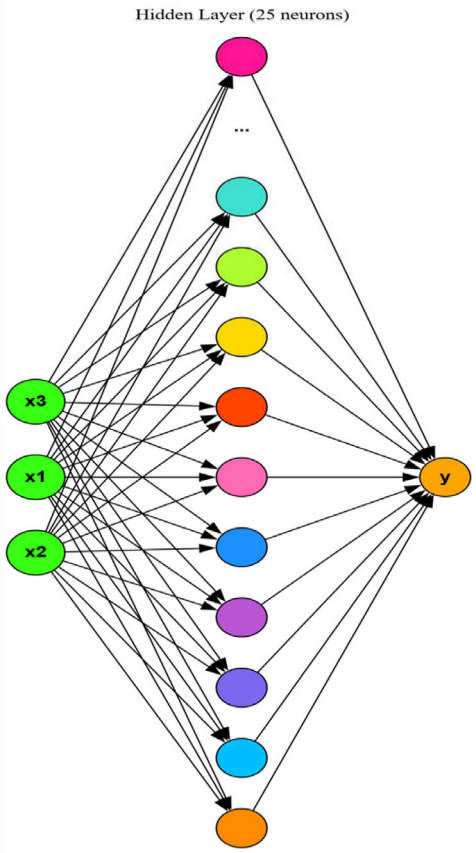

Fig. 1 ANN design and Categorize Data for Prediction.

The model was trained for up to 400 epochs with a batch size of 40. A 20% validation split is used to monitor performance on a subset of training data. The Early Stopping callback halts training if validation loss does not improve for 100 consecutive epochs, restoring the weights from the best epoch to prevent overfitting. This ensures the model balances learning and generalization. Furthermore, predictions are made on both training and test sets in the scaled [0, 1] range. In addition, these predictions are clipped to [0, 1] to respect the normalization bounds and then inverse-transformed with the scaler to return to the original data scale, making the results interpretable.

Model evaluation used metrics such as R^2, MSE, MAE, RMSE, MAPE, and bias, which show excellent predictive performance ($R^2 = 0.9946$).

Figs. 1 and 2 illustrate the ANN architecture and performance analysis. These scatter plots of actual versus predicted values for both the training and test sets, with fitted and ideal lines, illustrate prediction accuracy. Additionally, a line graph of absolute errors for test samples highlights prediction inaccuracies, and a histogram with a kernel density estimate (KDE) illustrates the distribution of prediction errors, providing insights into model bias and error patterns. This relatively high range of R^2 values (0.9946) enables us to use this correction factor in WR dual-porosity models to account for a geometrically complex fracture system.

Results and Discussion

The developed artificial neural network (ANN) was trained on an extensive dataset comprising 2,478 high-simulation samples generated through COMSOL Multiphysics, with the fracture aperture coefficient (η) as the target output parameter. This dataset systematically provides a range of reservoir conditions, fracture configurations, and petrophysical properties (Table 2), ensuring robust model generalization across varying fracture orientations, matrix block dimensions, and reservoir geometries encountered in naturally fractured reservoirs. Importantly, the relatively narrow range of η values (1–1.317) reflects physically realistic anisotropy effects rather than numerical artifacts, emphasizing the need for a regression model capable of resolving subtle but physically significant variations.

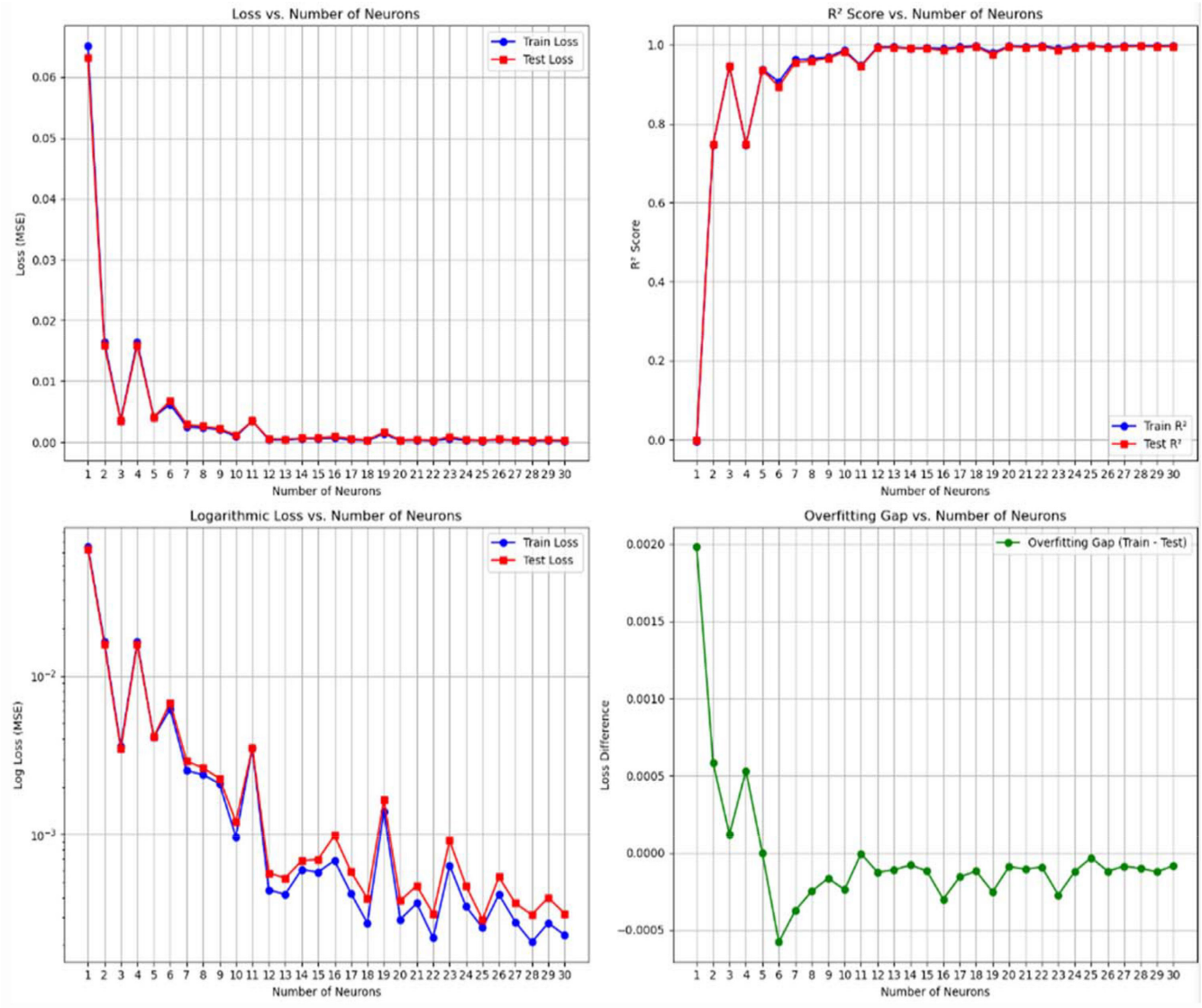

Fig. 2 Performance analysis with different neuron counts. Optimal performance achieved with 25 neurons, balancing model complexity and generalization ability. Shows loss values, R^2 scores, and overfitting gap across 1-30 neuron configurations.

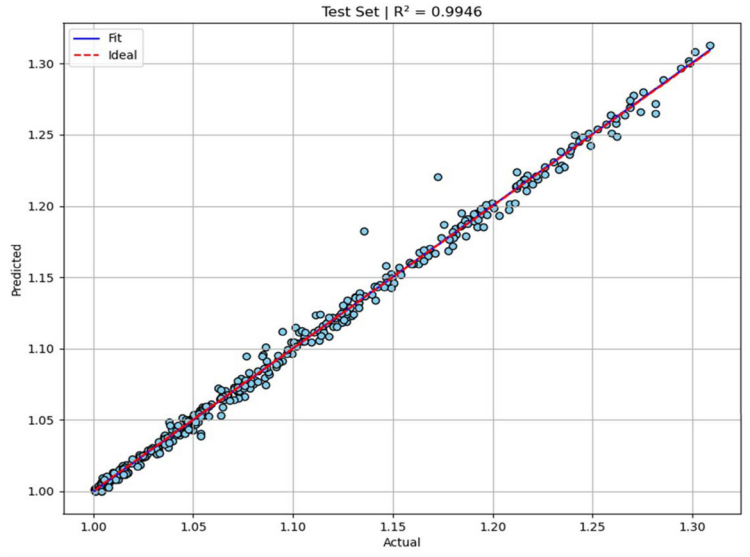

Fig. 3 Actual vs. Predicted Values for the Test Set (R^2 = 0.9946).

Table 2 Statistical Features of the 2478 Datasets used to Train AI Models for Fracture Aperture Correction Factor.

Parameter	Minimum	Maximum	Mean	Median	Var	SD
Matrix Area (m^2)	9.589	496.4	251.626	248.532	19381.4	139.217
Reservoir Area (m^2)	40.132	13968.201	2570.571	1877.008	5844620	2417.565
Fracture Degree (°)	5.425	89.958	48.953	48.938	585.438	24.196
Frac Aperture Coef	1	1.317	1.105	1.085	0.007	0.081

Evaluation of the trained ANN on an independent test dataset (15% of the whole) yielded a coefficient of determination (R^2) of 0.9946, indicating that the model successfully captures the dominant trends governing η. While high predictive accuracy alone does not guarantee physical validity, further analyses were conducted to assess the model's physical consistency, robustness, and interpretability. The high predictive accuracy (99.5%) was consistent with the training set performance (R^2 = 0.9959), confirming the model's ability to capture the complex non-linear mapping between input features and the fracture aperture correction coefficient while effectively mitigating overfitting concerns (as seen in Fig. 3).

Due to the cubic dependence of permeability on η, even marginal inaccuracies in η propagate into large errors in permeability estimation. For example, a 5% underestimation in η (e.g., predicting 1.05 instead of the true 1.10) can cause a permeability error exceeding 14%, severely affecting flow predictions. The high ANN accuracy mitigates this risk, providing more confident input parameters for simulation models. Moreover, the correction coefficient encapsulates the anisotropic permeability effects caused by fractures inclined at arbitrary angles θ relative to the flow direction. This allows for a realistic representation of fracture networks, which are seldom orthogonal or uniform in natural reservoirs.

Hence, by providing an accurate correction factor, the anisotropy caused by fracture orientation can be efficiently incorporated into conventional simulators, leading to more realistic predictions of:

• Pressure Transients: Well test analysis using a model with a corrected η will yield more accurate interpretations of fracture and matrix properties.

• Fluid Flow Paths: The flow of water or gas during injection processes will be more accurately modeled, improving predictions of breakthrough times and sweep efficiency.

• Ultimate Recovery: More accurate reservoir models, accounting for fracture orientation effects, provide better forecasts of oil recovery, optimizing field development planning.

The presented approach aligns with and extends prior research. The use of an equivalent aperture to account for anisotropy echoes the work of Zhang et al. [22] on coalbed methane reservoirs and the earlier propositions of Young et al. [21]. However, this study advances the field by shifting from a conceptual or analytical solution to a practical, generalized predictive tool based on machine learning.

Moreover, this research contributes to the growing application of AI in petroleum engineering, demonstrating that ANNs can go beyond mere pattern recognition to effectively learn underlying physical relationships in complex multiphase flow systems [32-33]. The ANN model acts as a surrogate for computationally intensive multiphase flow simulations, enabling integration into real-time decision support. This capability has a potential for coupling with dynamic reservoir management tools to optimize production in fractured formations.

Furthermore, this research contributes to the growing application of AI in petroleum engineering [32-33]. It demonstrates that ANNs can also learn the underlying physics of complex hydrodynamic problems, such as the relationship between fracture geometry and effective properties in multiphase flow systems. The model serves as a highly accurate and computationally efficient proxy for the numerical simulations, enabling rapid sensitivity analysis and uncertainty quantification that would be infeasible with full-physics models alone.

To evaluate the robustness of the ANN and mitigate concerns regarding overfitting to synthetic data, an extrapolation test was performed. The model was trained using samples with fracture angles between 10° and 70° and tested on an unseen angular range between 70° and 90°. The low MAPE value (<0.5%) underscores the ANN's practical reliability for industrial implementation, which is particularly critical in reservoir engineering applications, where even marginal prediction errors can propagate into substantial performance deviations during full-field simulations. Visual diagnostic plots reveal tightly clustered predictions around the ideal prediction line (y=x) with minimal scatter (Figs. 3 and 4), while residual analysis demonstrates a near-normal error distribution centered precisely at zero (Figs. 5 and 6). This statistical symmetry confirms the absence of systematic bias and highlights the purely stochastic nature of the residual errors, further validating the model's structural integrity.

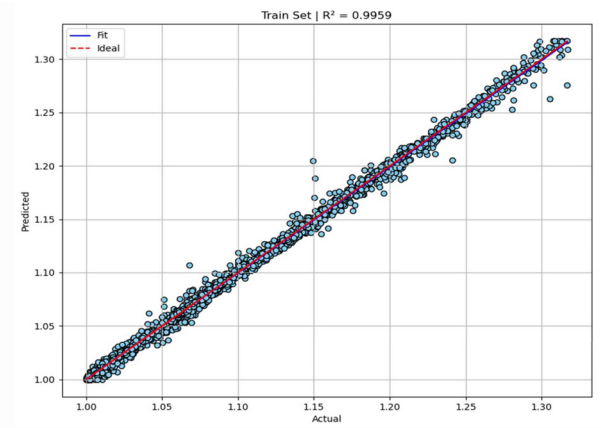

Fig. 4 Actual vs. Predicted Values for the Training Set ($R^2 = 0.9959$).

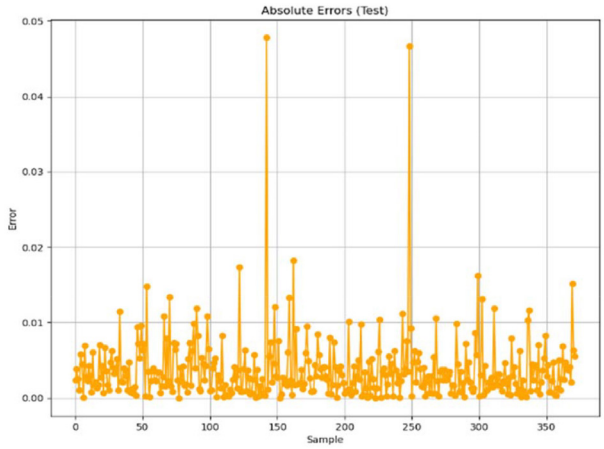

Fig. 5 Absolute Errors Distribution across Test Samples.

To assess the relative influence of input parameters on the predicted correction coefficient, a permutation-based feature importance analysis was performed. Moreover, this analysis quantifies *η's* sensitivity to perturbations in each input parameter while preserving the underlying data distribution. Moreover, the relative importance of input parameters, including: (1) Fracture Angle (θ), (2) matrix area and (3) reservoir area, for η prediction is shown in Table 3. Also, based on the study which was carried out, the amounts of relative importance for (1) fracture angle (θ), (2) matrix area and (3) reservoir area are 61%, 25% and 14%, respectively.

Table 3 Relative Importance of Input Parameters for η Prediction.

Input Parameter	Relative Importance (%)
Fracture Angle (θ)	61
Matrix Area	25
Reservoir Area	14

The results indicate that fracture orientation is the dominant factor for η, confirming that anisotropy effects are primarily governed by fracture geometry rather than reservoir size. This outcome aligns with physical expectations and supports the ANN's validity as a physics-consistent model.

The primary scientific contribution of this investigation is the development of a robust, data-driven methodology for accurately quantifying the equivalent fracture aperture correction coefficient (η). This parameter proves instrumental in transcending the limitations inherent in idealized "sugar cube" (Warren-Root) conceptual models by enabling precise representation of reservoirs characterized by non-orthogonal fracture networks.

Due to the cubic relationship between permeability and aperture ($k \alpha \eta^3$), even modest inaccuracies in η estimation propagate non-linearly into substantial errors in permeability prediction. For instance, a seemingly negligible 5% underestimation of η (e.g., predicting 1.05 instead of the actual 1.10) results in an approximately 14.3% error in permeability estimation, potentially leading to significant discrepancies in production forecasts. The exceptional accuracy of our ANN model mitigates the risk of cascading errors, providing substantially more reliable input parameters for multiphase flow simulation frameworks.

Moreover, the correction coefficient η elegantly encapsulates the complex anisotropic permeability effects induced by fractures inclined at arbitrary angles θ relative to the principal flow direction. In addition, this mathematical representation enables realistic characterization of natural fracture networks, which rarely conform to idealized orthogonal or uniform configurations in subsurface formations.

Hence, by providing an accurate correction factor, the anisotropy resulting from fracture orientation can be effectively incorporated into conventional simulators, leading to more realistic predictions of pressure transients (i.e. well test analysis using a model with a corrected η will yield more accurate interpretations of fracture and matrix properties), fluid flow paths (i.e. flow of water or gas during injection processes will be more accurately modeled, improving predictions of breakthrough times and sweep efficiency) and ultimate recovery (i.e. more accurate reservoir models, accounting for fracture orientation effects, provide better forecasts of oil recovery, optimizing field development planning).

The presented approach both aligns with and substantially extends previous research initiatives in this domain. The use of equivalent-aperture concepts to address anisotropy aligns with the methodological framework proposed by Zhang et al. [22] for coalbed methane reservoirs and builds upon the foundational theoretical work of Young et al. [21]. However, this investigation advances the scientific frontier by transcending purely conceptual or analytical solutions, instead providing a practical, generalized predictive tool through sophisticated machine learning implementation.

This research makes a significant contribution to the expanding integration of artificial intelligence in petroleum engineering applications [32-33]. It convincingly demonstrates that properly designed neural networks can progress beyond pattern recognition to effectively capture the underlying physics of complex hydrodynamic systems, specifically the intricate relationship between fracture geometry and effective flow properties in multiphase transport processes. The developed ANN model functions as a computationally efficient surrogate for resource-intensive numerical simulations, enabling:

• Accelerated Sensitivity Analysis: Rapid exploration of fracture geometry effects on multiphase flow behavior without the computational burden of full-physics simulations.

• Comprehensive Uncertainty Quantification: Systematic assessment of prediction confidence intervals and associated risk mitigation strategies in fractured reservoir management.

• Real-time Decision Support Integration: Potential for seamless coupling with dynamic reservoir management platforms to optimize production strategies in complex naturally fractured formations.

The exceptional predictive accuracy achieved (MAPE < 0.5%) positions this methodology as a valuable addition to the reservoir engineer's analytical toolkit, bridging the persistent gap between idealized conceptual models and the complex reality of naturally fractured reservoir systems.

Conclusions

This study advances the characterization and modeling of anisotropic fractured media by introducing a physics-informed, data-driven framework to quantify the fracture aperture correction coefficient (η). By treating η as a functional response to fracture orientation, matrix shape, and reservoir geometry rather than a constant calibration parameter, the proposed approach bridges fracture-scale flow physics and continuum dual-porosity modeling.

The ANN model performed very well, achieving high predictive accuracy (R^2 = 0.9946, MAPE = 0.34%) while preserving physical consistency, as confirmed by sensitivity, partial dependence, and extrapolation analyses. The results show that fracture orientation is the dominant control on η and that accurate estimation of this parameter significantly reduces permeability uncertainty arising from the cubic aperture–permeability relationship.

By incorporating this correction factor into the Warren–Root framework, the applicability of conventional dual-porosity models is extended to reservoirs with non-orthogonal fracture networks. The proposed methodology provides a computationally efficient and physically interpretable tool for improving (1) flow prediction, (2) well test analysis, and (3) reservoir management decisions in naturally fractured systems.

In this study, we focused on fracture orientations, fracture size, and system size. Further studies are needed to consider the effects of other factors, including stress-aperture relation, aperture variations, and roughness within single fractures, to propose a more general approach for estimating equivalent aperture in flow simulations to avoid errors in both principal permeabilities and flow patterns.

Nomenclatures

H: Fracture aperture correction coefficient –
Φ: Porosity (Fraction)
K: Permeability m^2
M: Fluid viscosity (Pa·s)
P: Fluid density (kg/m^3)
Q: Source or sink term (m3/s)
G: Gravitational acceleration (m/s^2)
Z: Depth (m)
∇: Gradient operator (–)
Θ: Fracture inclination angle (°)
T: Transmissibility coefficient (–)
Sα: Phase saturation (α = water, oil) (–)
Φ: Flow potential (–)
ANN: Artificial Neural Network (–)
WR: Warren–Root dual-porosity model (–)
DFN: Discrete Fracture Network (–)
COMSOL: COMSOL Multiphysics software (–)
R^2: Coefficient of determination (–)
MAPE: Mean Absolute Percentage Error (%)
KDE: Kernel Density Estimate (–)

References

1. Saeedi, M. (2016). Application of Multi-Stage Fracturing of Horizontal Wells in SAGD Technology (Doctoral dissertation, University of Calgary (Canada)).
2. Nelson, R. A. (1985). Geologic analysis of naturally fractured reservoirs (Vol. 1). Gulf Professional Publishing.
3. Allen, P. A., & Allen, J. R. (2013). Basin analysis: Principles and application to petroleum play assessment. John Wiley & Sons.
4. Narr, W., Schechter, D. S., & Thompson, L. B. (2006). Naturally fractured reservoir characterization. (No Title).
5. Dershowitz, W. S., & Einstein, H. H. (1988). Characterizing rock joint geometry with joint system models. Rock mechanics and rock engineering, 21(1), 21-51.
6. Aguilera, R. (1995). Naturally fractured reservoirs (2nd ed.). PennWell Books.
7. Bear, J. (1972). Dynamics of fluids in porous media. Elsevier.
8. Reiss, L. H. (1980). The reservoir engineering aspects of fractured formations. Editions Technip.
9. Lucia, F. J. (1995). Rock-fabric/petrophysical classification of carbonate pore space for reservoir characterization. AAPG bulletin, 79(9), 1275-1300.
10. Aguilera, R. (2002). Incorporating capillary pressure, pore throat aperture radii, height above free-water table, and Winland r 35 values on Pickett plots. AAPG bulletin, 86(4), 605-624. doi.org/10.1306/61EEDB5C-173E-11D7-8645000102C1865D.
11. Corey, A. T. (1977). Mechanics of heterogeneous fluids in porous media (pp. 259-pp). ISBN (Hardback): 978-0-918334-17-6.
12. Parsons, R. W. (1966). Permeability of idealized fractured rock. Society of Petroleum Engineers Journal, 6(02), 126-136. doi.org/10.2118/1289-PA.
13. Long, J. C., Remer, J. S., Wilson, C. R., & Witherspoon, P. A. (1982). Porous media equivalents for networks of

discontinuous fractures. Water resources research, 18(3), 645-658. doi.org/10.1029/WR018i003p00645.
14. Dershowitz, W., & Miller, I. (1995). Dual porosity fracture flow and transport. Geophysical Research Letters, 22(11), 1441-1444. doi.org/10.1029/95GL01099.
15. Barenblatt, G. I., Zheltov, Y. P., & Kochina, I. N. (1960). Basic concepts in the theory of seepage of homogeneous liquids in fissured rocks. Journal of Applied Mathematics and Mechanics, 24(5), 852-864.
16. Warren, J. E., & Root, P. J. (1963). The behavior of naturally fractured reservoirs. Society of Petroleum Engineers Journal, *3*(3), 245–255.
17. Kazemi, H. (1969). Pressure transient analysis of naturally fractured reservoirs with uniform fracture distribution. Society of Petroleum Engineers Journal, *9*(4), 451–462.
18. de Swaan, A. (1990). Analytic solutions for determining naturally fractured reservoir properties by well testing. Society of Petroleum Engineers Journal, *30*(3), 479–486.
19. Gerke, H. H., & van Genuchten, M. T. (1993). A dual-porosity model for simulating the preferential movement of water and solutes in structured porous media. Water Resources Research, *29*(2), 305–319.
20. Zimmerman, R. W., Chen, G., Hadgu, T., & Bodvarsson, G. S. (1993). A numerical dual-porosity model with semianalytical treatment of fracture/matrix flow. Water Resources Research, 29(7), 2127–2137.
21. Young, R. A., Randolph, P. L., & Lee, W. J. (1989). Application of the equivalent fracture aperture in the Warren-Root model. SPE Formation Evaluation, 4(2), 233–240.
22. Zhang, Z., Li, X., & Wang, X. (2022). Improved permeability model with equivalent fracture aperture for coal anisotropy. International Journal of Coal Geology, *261*, 104077.
23. Geiger, S., & Matthäi, S. K. (2012). What can we learn from high-resolution numerical simulations of single- and multi-phase fluid flow in fractured outcrop analogues? Advances in Water Resources, 51, 220–236.
24. Tryggvason, G., Bunner, B., Esmaeeli, A., Juric, D., Al-Rawahi, N., Tauber, W., Han, J., Nas, S., & Jan, Y. J. (2001). A front-tracking method for the computations of multiphase flow. Journal of Computational Physics, 169(2), 708–759.
25. Hirt, C. W., & Nichols, B. D. (1981). Volume of fluid (VOF) method for the dynamics of free boundaries. Journal of Computational Physics, *39*(1), 201–225.
26. Osher, S., & Sethian, J. A. (1988). Fronts propagating with curvature-dependent speed: Algorithms based on Hamilton-Jacobi formulations. Journal of Computational Physics, 79(1), 12–49. doi: 10.1016/0021-9991(88)90002-2.
27. Sussman, M., Smereka, P., & Osher, S. (1994). A level set approach for computing solutions to incompressible two-phase flow. Journal of Computational Physics, 114(1), 146–159. doi: 10.1006/jcph.1994.1155
28. Guadala, A., Dvorkin, J., & Mavko, G. (2020). Coupled hydro-geomechanical modeling of fractured reservoirs. Journal of Geophysical Research: Solid Earth, *125*(7), e2020JB019587.
29. Kumar, A., Ozkan, E., & Gokaraju, B. (2016). Simulation of viscous fingering in homogeneous porous media using COMSOL. In COMSOL Conference.
30. Patani, P., Smith, R., & Kumar, A. (2023). Probabilistic assessment of equivalent fracture aperture constrained by real-time drilling mud loss data. Journal of Petroleum Science and Engineering, 224, 111234.
31. Zhou, Y., Wang, X., & Li, Q. (2023). Phase-field modeling of fluid-driven dynamic crack propagation in porous media using COMSOL Multiphysics. International Journal of Rock Mechanics and Mining Sciences, 168, 105401.
32. El Ouahed, A. K., Tiab, D., & Mazouzi, A. (2005). Application of artificial intelligence to characterize naturally fractured zones in Hassi Messaoud oil field, Algeria. Journal of Petroleum Science and Engineering, 49(3–4), 122–141. doi: 10.1016/j.petrol.2005.05.003.
33. Al-Dhamen, M., Al-Mulhem, A., & Al-Yami, A. (2021). AI-based model for predicting acid fracturing performance in naturally fractured reservoirs. Journal of Petroleum Science and Engineering, 196, 107689.
34. Peng, C., Zhang, L., & Li, X. (2019). Integration of EDFM and AI for history matching in fractured reservoirs. Journal of Natural Gas Science and Engineering, 71, 102982.
35. Kumar, S., Ghassemi, A., & Pandey, V. (2023). Integration of SVM and neural networks for natural fracture characterization in shale gas reservoirs. Fuel, *332*, 126112.
36. Zheng, S., Li, H., & Zhang, T. (2022). Coupling reservoir simulation with AI for fracture property optimization in shale gas sweet spot prediction. Energy, 239, 122345. doi.org/10.1016/j.energy.2021.122345.
37. Alqahtani, A., Khan, M. A., & Al-Hajri, M. (2023). Application of random forests and neural networks for predicting fluid loss and complex flow behavior in fractured reservoirs. Journal of Petroleum Exploration and Production Technology, 13(2), 451–463.
38. Al-Sulaiman, S., Rahman, M., & Al-Shammari, H. (2023). Machine learning investigation of single fracture influence on flow dynamics in dolomite formations. Energy Reports, 9, 788–799.
39. Hassan, A., Mohebian R. (2023). Machine learning applications in fractured reservoir characterization. Journal of Petroleum Technology. doi.org/10.1016/j.ptlrs.2025.04.006.
40. Bian, X., Zhou, J., Fu, L., Jin, A., Gorelick S., & Zhang, W. (2026). Artificial Intelligence for Hydraulic Fracturing Decision Support: A Workflow-Oriented Critical Review. Processes, 14(16), 2537-2546. doi.org/10.3390/pr14162537.
41. Nick, H. M., & Bisdom, K. (2018, February). Fracture aperture in flow models: to average, or not to average?. In Third EAGE Workshop on Naturally Fractured Reservoirs. 2018, 1, 1-4. European Association of Geoscientists & Engineers. doi.org/10.3997/2214-4609.201800028.
42. Hu, M., & Rutqvist, J. (2022). Multi-scale coupled processes modeling of fractures as porous, interfacial

and granular systems from rock images with the numerical manifold method. Rock Mechanics and Rock Engineering, 55(5), 3041-3059. doi.org/10.1007/s00603-021-02455-6.

43. Luo, B., & Wong, G. K. (2024, June). Enhancing Cluster Efficiency by Modeling Swelling Diverter Particles in PKN-Type Fractures. In ARMA US Rock Mechanics/Geomechanics Symposium (p. D031S027R002). ARMA.
44. Yang, Z., Li, D., Xue, S., Hu, R., Gorelick S. & Chen, Y. F. (2019). Effect of aperture field anisotropy on two-phase flow in rough fractures, Advances in Water Resources, 132, 103390-103397, doi.org.10.1016/j.advwatres.2019.103390.
45. Kim, S., Lee, J. (2024). Dual-porosity modeling improvements for anisotropic fractured reservoirs. SPE Journal.
46. Goodfellow, I., Bengio, Y., & Courville, A. (2016). Deep learning. MIT Press.
47. Mohaghegh, S. (2000). Virtual-intelligence applications in petroleum engineering: Part 1—Artificial neural networks. Journal of Petroleum Technology, *52*(9), 64–73.
48. Ouenes, A., Bhagavan, S., & Bunge, R. (1995). Application of neural networks in petroleum engineering. SPE Computer Applications, 7(2), 42–48.